A high frequency amplitude-steered array for real-time volumetric imaging

Catherine H. Frazier[a)]
Bioacoustics Research Laboratory, Department of Electrical and Computer Engineering, University of Illinois at Urbana-Champaign, Urbana, Illinois 61801

W. Jack Hughes[b)]
Applied Research Laboratory, The Pennsylvania State University, P.O. Box 30, State College, Pennsylvania 16801

William D. O'Brien, Jr.[c)]
Bioacoustics Research Laboratory, Department of Electrical and Computer Engineering, University of Illinois at Urbana-Champaign, Urbana, Illinois 61801

(Received 12 August 2000; revised 13 June 2002; accepted 26 June 2002)

Real-time three-dimensional acoustic imaging is difficult in water or tissue because of the slow speed of sound in these media. Conventional pulse–echo data collection, which uses at least one transmit pulse per line in the image, does not allow for the real-time update of a volume of data at practical ranges. Recently, a linear amplitude-steered array was presented that allows the collection of a plane of data with a single transmit pulse by spatially separating frequencies in the lateral direction. Later, by using a linear array with frequency separation in the vertical direction and rotating the array in the horizontal direction, volumetric data were collected with a small number of transmit pulses. By expanding the linear array to a two-dimensional array, data can now be collected for volumetric imaging in real time. In this study, the amplitude-steered array at the heart of a real-time volumetric sonar imaging system is described, giving the design of the array and describing how data are collected and processed to form images. An analysis of lateral resolution in the vertical and horizontal directions shows that resolution is improved in the direction of frequency separation over systems that use a broad transmit beam. Images from simulated data are presented.
 [DOI: 10.1121/1.1518699]

PACS numbers: 43.30.Yj, 43.30.Wi [DLB]

I. INTRODUCTION

The concept of steering the maximum response of an array using amplitude weighting was introduced by Hughes and Thompson in 1976.[1] At that time, the intent of amplitude steering was to steer the maximum response of the beam patterns without using phase-shift networks or multiple delay lines. Initially, amplitude weighting was applied with an electronic gain.[2] When large-area transducer material became available, shaped hydrophones were developed where shading for low sidelobes was achieved geometrically.[3,4] It was realized that in addition to the low sidelobes, geometrical amplitude steering could also be used to form a set of steered beams. In the original concept, the beam was steered to a particular direction at a single frequency, and the fact that the steering direction changed with frequency was considered a drawback of the design. With the availability of broadband large-area 1–3 composite material, a transducer array was built which could form multiple beams at multiple frequencies.[5] The imaging concept was introduced when it was realized that a single FM pulse could be used to sweep the maximum response axis over a range of steering angles. A plane of data is created from a single receive signal using a short-time Fourier transform (STFT) where the frequencies contained within the window give the azimuth of the targets and the temporal position of the STFT window gives the range of the targets. Three-dimensional acoustic imaging is an extension, where beams in the orthogonal plane are obtained by mechanical or time-delay steering. The potential advantages of using the amplitude weighting for steering and imaging are greatly reduced size of the electronics and high frame rate volumetric imaging.

Volumetric acoustic imaging has received attention recently for both sonar and medical applications because it allows better visualization of structures or anatomy than a series of two-dimensional slice images. Real-time volumetric imaging, meaning updating the volume of data at a rate of at least 30 Hz, is even more valuable. In sonar, volumetric imaging is most often considered for short-range applications (less than 10 meters) such as fish counting, assisting divers, monitoring remotely operated vehicles, or mine hunting. Real-time three-dimensional imaging could provide the visibility required for a diver to locate objects such as damaged pipes in turbid water. In medical imaging, three-dimensional images could provide information on the shape of a solid mass, one of the parameters used to distinguish between benign and malignant tumors. Real-time three-dimensional im-

[a)]Electronic mail: hillsley@brl.uiuc.edu. Current address: Johns Hopkins University Applied Physics Laboratory, 11100 Johns Hopkins Road, Laurel, MD 20723.
[b)]Electronic mail: wjh2@psu.edu
[c)]Electronic mail: wdo@uiuc.edu

aging would allow a physician to view the structures of the heart throughout the cardiac cycle.

Data collection for a three-dimensional image using techniques of two-dimensional imaging requires too much time for volumes to be scanned in real time. Although the speed of sound is similar for sonar and medical applications, the maximum ranges of interest are very different. Collecting data for a two-dimensional medical image with a maximum range of 20 cm requires 25 ms, where the speed of sound is assumed to be 1540 m/s and where 128 pulses are used to create 128 lines in the image. A three-dimensional image formed with 128^2 pulses under the same conditions requires 3.19 seconds. Real-time three-dimensional imaging using conventional data collection techniques would be impossible. For sonar imaging, with a maximum range of 5 m and a speed of sound of 1500 m/s, transmitting and receiving a single pulse requires 6.7 ms. No more than 5 pulses could be used to scan the volume in real time.

A solution to this problem is to form several receive beams for one transmitted pulse and to separate reflections from different directions through processing. Several other groups have worked on developing such techniques in both sonar and medicine. Sonar systems were discussed in Ref. 5. Three-dimensional medical ultrasound exists; however, with one exception, it is not real time. Currently available systems typically scan two-dimensional planes using linear arrays and then translate or rotate the array to scan the next plane. Three-dimensional images are then formed off-line.[6] For cardiac imaging, where real-time data collection is most critical, data are often collected over several heart beats, and then the data from different cycles are combined so that a single heart cycle can be recreated as a cineloop. Successive heart beats must be similar enough for the reconstruction. In many cases, irregular heart beats are thrown out,[7,8] making it impossible to use these systems to diagnose a heart abnormality.

Researchers from Duke University have a real-time volumetric imaging system, which is in operation.[9] Their system uses a sparse, two-dimensional array. As reported in 1991, the volume is scanned in a pyramidal scheme, with 12 transmit pulses in the elevation direction and 52 transmit pulses in the azimuthal direction, for a total of 624 transmit pulses per volume. Parallel beamforming is used in the elevation direction so that eight receive beams are formed for each transmit pulse. The volume can be scanned eight times per second. Initial image quality was poor. To improve the image quality, they have been working on improving the two-dimensional array, increasing channel count and frequency. Their method is unsuitable for sonar because of the large number of transmitted pulses used.

Lu[10] has proposed a technique for three-dimensional imaging using limited diffraction beams. A plane-wave pulse is transmitted from the two-dimensional array to illuminate the scene. In reception the same transducer array is used to form an array of limited diffraction beams by weighting the elements of the array. A complete data set is formed by varying the element weighting. Using a three-dimensional inverse Fourier transform, a three-dimensional image is created. This technique requires a fairly large, broadband array. The largest cross-sectional area that can be imaged without greatly reducing the speed of data collection is equal to the area of the array. The method has been tested using a phantom with embedded point scatterers.[11] The results look promising, although the images reveal the dependence of the technique on the broad bandwidth of the transducer.

Shen and Ebbini[12] have worked on coded excitation in combination with a pseudoinverse operator so that multiple beams from different steering directions can be received at one time. Independent codes are transmitted on each element, resulting in different impulse responses in each steering direction. Returns from different directions are then separated using pseudoinverse filters. The number of beams that can be formed simultaneously depends on the number of filters in the filter bank. Previous images formed using coded-excitation methods with matched filter operators have suffered because correlations between beams in different directions produce artifacts in the images. Shen and Ebbini's technique is reported not to have this drawback; however, the pseudoinverse operator suffers from consequences of the assumption that targets occur on a grid pattern. If target positions differ from the grid pattern, the image quality is degraded.

We are interested in a real-time sonar system with high resolution. Our current application is a diver-held sonar system intended for real-time detection and identification of submerged mines. We expect the mines to be metallic or plastic targets suspended in water or sitting on the soft bottom of the water body, with characteristic dimension of 50 cm and features on the order of 1 cm. The goal is to image a volume from 3 to 5 meters in front of the array, with a resolution voxel of 1 cm. The imaged volume is 20° wide in the vertical direction and 30° wide in the horizontal direction. The resolution requirement leads to the choice of 1 to 5 MHz as the desired operating frequency range. Current volumetric sonar systems have low resolution due to the broad transmit beam. As discussed above, medical systems use too many transmit pulses to be adapted for sonar, or they have other drawbacks. Our solution is to extend the amplitude-steered array for real-time volumetric sonar imaging. Our system could also work for medical imaging; however, in that case we might make different choices for operating frequency and array dimensions.

In Ref. 5, the linear amplitude-steered array was used for volumetric imaging by rotating the array. A plane of data was collected with each transmit pulse. However, the rate of data collection can be increased by using a transmit beam that is narrow and steered in the vertical direction and broad in the horizontal direction.

In order to image a volume of interest with a single transmit pulse, the received signal must contain information to give vertical, horizontal, and range position of the target. The linear-phased amplitude-steered array uses frequency separation to determine vertical position and conventional beamforming to determine horizontal location. The range of the target is obtained from the time elapsed until the reflected signal is received. The vertical position information is determined by the frequency of the returned signal. The horizontal position of the target is found by using conventional, linear

phased array processing of the signals from the *staves* or columns of elements.

In Sec. II, we describe the new array layout for achieving amplitude steering, which results in lower peak sidelobe levels than the previous design. In Sec. III, we discuss the procedure for data collection and the algorithms for image formation including time–frequency processing beyond the STFT. In Sec. IV, we describe simulations and show resulting images. In addition, we compare resolution results in the vertical and horizontal lateral directions. Section V discusses the relationship between the amplitude-steered array and Lu's imaging with nondiffracting beams. Finally, we give a conclusion.

II. ARRAY LAYOUT AND BEAM PATTERN

Amplitude steering has been described in detail previously (see Ref. 1), so we limit this discussion to changes in the array design. Amplitude steering in the vertical direction is achieved by applying weights to each row. [The weights are $\cos\{(2n-1)\phi\}$, $\sin\{(2n-1)\phi\}$, where n is the row number, $\phi=(k_0 d/2)\sin\theta_0$, k_0 is the wave number at the design frequency, d is the row spacing, and θ_0 is the design steered angle.] Weights are applied geometrically, not by scaling the signals, but by grouping elements together. Earlier versions of the amplitude-steered array assigned elements to sine and cosine regions by trying to match regions that would be created for a shaped PVDF transducer. This array layout produced undesirable peak sidelobe levels. For the linear-phased amplitude-steered array, weighting is still applied by dividing the available area into regions; however, now the division is done on a row-by-row basis. The sine and cosine weightings are implemented by selecting the number of elements in each row that are connected together as sine or cosine elements. The signals from the sine elements must pass through an additional 90° phase shift before summing.

Each active element of a row must be assigned to the cosine or sine group such that the proper $\cos((2n-1)\phi)$ and $\sin((2n-1)\phi)$ row weightings are maintained. The numbers of each type of element in a row are determined by the equations

$$N_C(n)=\frac{N_n^{\max}}{1.414}\left|\cos\left((2n-1)\frac{k_0 d}{2}\sin\theta_0\right)\right|, \tag{1}$$

$$N_S(n)=\frac{N_n^{\max}}{1.414}\left|\sin\left((2n-1)\frac{k_0 d}{2}\sin\theta_0\right)\right|, \tag{2}$$

where N_C is the number of cosine elements, N_S is the number of sine elements, $N_n^{\max}$ is the maximum number of elements in the nth row, d is the spacing between the rows, k_0 is the design wave number, and θ_0 is the design steering angle in the vertical direction. For a rectangular array, $N_n^{\max}$ would be a constant for all n. For our array, which has a circular aperture, $N_n^{\max}$ depends on the row number. The $\cos((2n-1)\phi)$ and $\sin((2n-1)\phi)$ terms may represent positive or negative values. Thus, there are four element assignments: positive and negative cosine, and positive and negative sine. In each row, there are either positive cosine or negative cosine elements, not both. Also, there are either positive sine or negative sine elements, not both. We refer to elements by their group, e.g., cosine elements or sine elements.

The optimal beam pattern is that of an electronically steered array of the same size. The electronic phase gives each element both a cosine weight and a sine weight. For the amplitude-steered array, each element can contribute to either the cosine or the sine weighting, but not to both; therefore, we are essentially designing two sparse arrays, one cosine and one sine array.

An alternating element design, in which elements of the cosine and sine groups are alternated until $2\times\min(N_C,N_S)$ is reached, leads to high grating lobes in the horizontal direction at positions corresponding to an interelement spacing of $2d$. The positioning of the elements within the row was made random to avoid grating lobes. Patterns of random sparse arrays are characterized by a sidelobe pedestal level. The average sidelobe level of the intensity pattern is approximately N^{-1}, where N is the number of elements in the array.[13,14] Steinberg analyzed and compared the peak sidelobe level of sparse arrays designed using algorithmically aperiodic arrays and random placement of elements. He found that both produced the same mean peak sidelobe level, but that the variance of the random arrays was much smaller than that of algorithmically designed arrays, when all algorithmically designed arrays were compared as a group regardless of design method.

The random design was implemented as follows. Each element of the array was given a probability of being a cosine element and a probability of being a sine element, where the probabilities depended on the row of the array. The sum of these probabilities does not equal 1 for every row; therefore, it is also possible for the element to be nulled, or not used, in order to keep the proper relative row weighting for steering. A random number generator was used to assign element type. Figure 1 shows the array layout used for the simulations. Part (b) of the figure gives an expanded view of the region indicated by the white box in part (a). In the figure, there are five gray-scale levels for the four element assignments and the null elements. In each row there is a maximum of three gray-scale levels: one cosine, one sine, and one for the null elements. Figure 2 shows the beam pattern produced. The random array design produced a beam pattern whose main lobe has the same width as the main lobe of the full array, and the random array has no grating lobes or large sidelobes. The predicted average sidelobe level using Steinberg's expression is -51.12 dB. The average sidelobe level in the figure is approximately -44 dB. The peak sidelobe level is only 2.3 dB above the mean.

One potential advantage of using this array for volumetric imaging is the reduced electronics requirement compared to proposed array systems that must address each element individually. For the amplitude-steered array, a separate channel is not required for each element. Only four channels are required per stave. One channel is assigned for each element type: positive cosine, negative cosine, positive sine, and negative sine. The number of wires that must connect the array elements to the processor is also reduced, thereby reducing the required cable size.

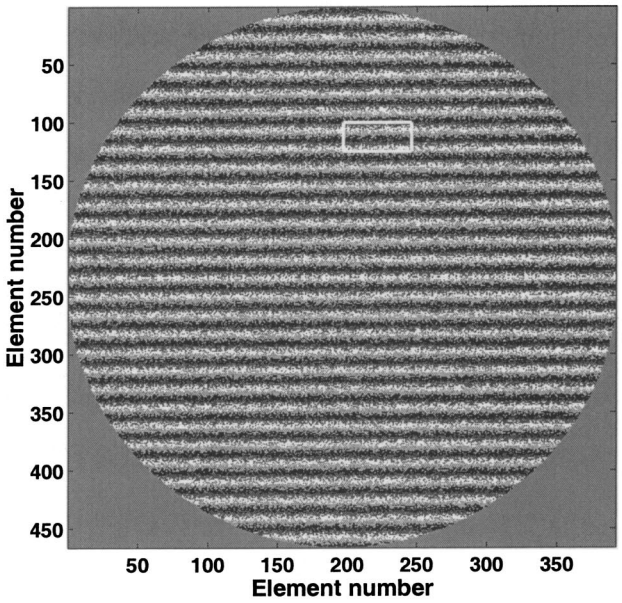

(a)

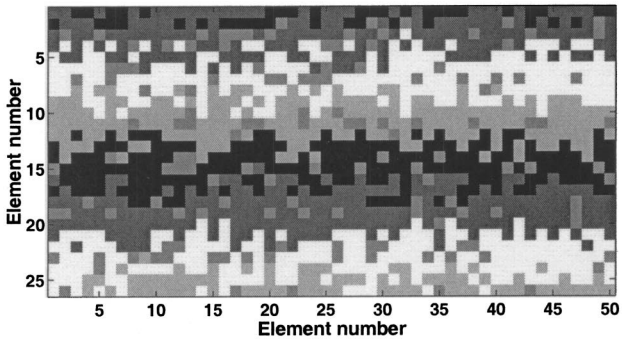

(b)

FIG. 1. (a) Array layout for 2D array with random placement of the four element phases. Four gray-scale levels represent the four phases of elements: white, cosine; black, negative cosine; light gray, sine; dark gray, negative sine. (b) Zoom of (a) to show detail. Isolated gray squares within more continuous regions indicate null elements.

III. DATA COLLECTION AND IMAGE FORMATION

Real-time data collection with the linear-phased amplitude-steered array is accomplished as follows. A linear FM chirp pulse is transmitted from the center two staves, which means that at a given frequency, the transmitted beam is wide in the horizontal direction and narrow in the vertical direction. The narrow beam in the vertical direction results in better resolution than current sonar systems that use a broad transmit beam in all directions. Frequencies are separated in the vertical direction with high frequencies steered deeper than low frequencies.

The reflected signal is received by the whole array. Signals from individual staves are digitized separately and are stored for further processing. Following the data collection, forming the complete three-dimensional data set consists of two steps. First, the signals from individual staves must be processed to give horizontal position information. Second, time–frequency processing is performed on signals corresponding to each horizontal steering direction to give vertical position and range information.

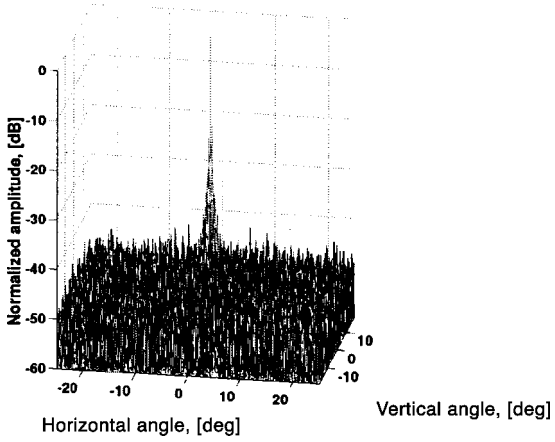

FIG. 2. Field pattern for array with random placement of elements.

A. Horizontal position information

The raw signals from individual staves are processed to give horizontal position information. The focusing delays do not change with horizontal steering direction, so they are applied first. The output from the array, with focusing delays applied, is a two-dimensional matrix with stave number along one direction and time sample number along the other. Then beam steering is accomplished using the Radon transform. The discrete Radon transform sums through a matrix at different angles, resulting in beams steered to several directions.[15]

Once the Radon transformation is complete, the two-dimensional data matrix contains one time signal for each horizontal steering direction. For a complete set of volumetric data, we then apply time–frequency processing to the time signal from each horizontal steering direction.

B. Time–frequency processing

Range and vertical position information are determined using time–frequency processing. Time resolution corresponds to range resolution and frequency resolution corresponds to vertical resolution for our application. Time–frequency processing has been used to identify targets in sonar signals based on characteristics of the received signals,[16,17] but has not been used to form an image of targets until Ref. 5.

We limit ourselves to Cohen's class of time–frequency distributions whose kernels are independent of the signal. Cohen's class of distributions is bilinear in the signal, and therefore is characterized by oscillating cross terms.[18] In this study, we implement two members of Cohen's class: the spectrogram, which is the magnitude squared of the short-time Fourier transform, and the smoothed pseudo-Wigner distribution (SPWD). The spectrogram is the most likely to be implemented for early arrays; however, with the spectrogram, there is a trade-off in time- and frequency resolution that depends on the length of the filter used. In an earlier study, an analysis of resolution using different time–frequency distributions to form images of point targets with the linear array showed that the SPWD gave the best overall results in terms of cross-term level and resolution in the

time- and frequency directions.[19] Of the distributions considered in that study, the SPWD had the most parameters available for optimization, allowing independent smoothing in the time- and frequency directions.

For the current study, parameters such as the filter lengths and shapes were determined by forming images of point targets and optimizing those images for visual appearance. The final window for the spectrogram was chosen to be a Hanning window with a length of 1024 samples or 50 μs. For the SPWD, the filters used for smoothing in the time and frequency directions were Gaussian windows, described by the expression $\exp(-t^2/\alpha^2-\omega^2/\beta^2)$, where α is 3.4 μs and β is 125.7×10^3 rad/s.

The result of time-frequency processing is a three-dimensional data set, where for each horizontal steering direction, vertical position and range have been obtained.

C. Resolution

The image resolution is dependent not only on the size of the array, but also on the processing used to form the images.[20] First, we describe the resolution that is achievable by the array, without considering the processing. Then, we will consider the resolution obtained when using the spectrogram or SPWD. Range resolution will be given in millimeters. It is dependent on the bandwidth of the received signal and the size of the array, as in the case of the linear amplitude-steered array. Vertical and horizontal resolutions are measured in degrees. In the vertical direction, the lateral resolution is very much like that of the linear amplitude-steered array, which is described in Ref. 20. The resolution will get worse as the vertical angle increases because the high frequencies are steered downward. In the horizontal direction, the resolution is similar to that of an electronically phased array.

The theoretical description of resolution is complicated by the multiple frequencies and multiple foci in the horizontal direction. For the lowest frequencies used, the volume of interest is in the far field; therefore, focusing will not be effective. Horizontal resolution could be estimated by determining the far-field beam spread of the array. For the highest frequencies, the region of interest is in the near field. Six different focal regions are used. A theoretical value for horizontal resolution can be determined at the location of the foci. At other locations, the diffraction-limited spreading must be taken into account. Vertical resolution depends on the frequency separation. Resolution is investigated through simulations because of the many different cases within our volume of interest.

IV. SIMULATIONS AND RESULTS

The operation of the linear-phased amplitude-steered array for imaging and the results of projection images are demonstrated through simulation.

A. Processing

Data collection with the random two-dimensional amplitude-steered array is simulated using the FIELD II program by Jensen.[21,22] A block diagram of the simulations is shown in Fig. 3. Data collection was simulated in four parts: cosine elements transmitting, cosine elements receiving; cosine elements transmitting, sine elements receiving; sine elements transmitting, cosine elements receiving; and sine elements transmitting, sine elements receiving.

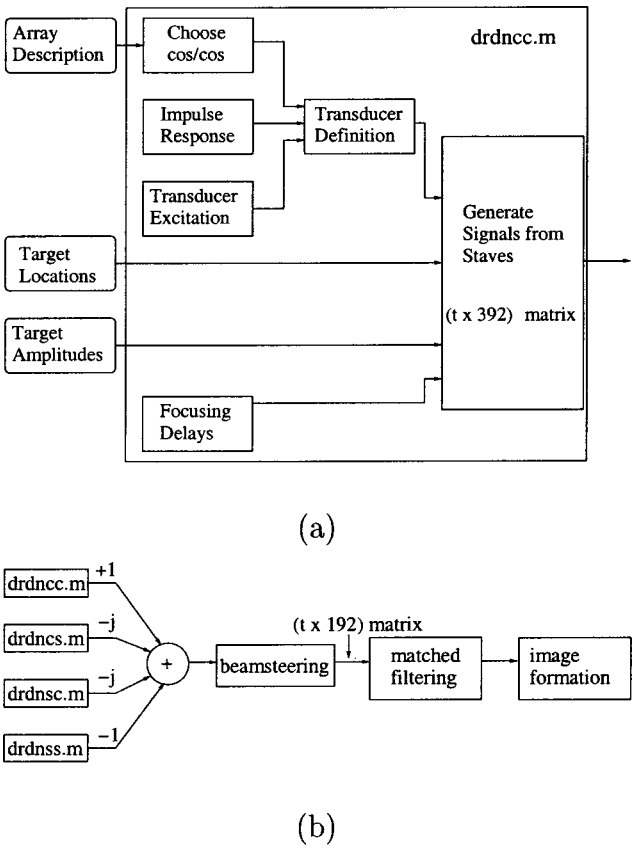

FIG. 3. Block diagram of simulation. The variable t in the matrix sizes indicates the number of time samples received, which depends on the distance between the closest and farthest point targets and the sampling rate.

Part (a) of Fig. 3 shows the diagram for one of the four parts. The array description, frequency response of the transducer, point target locations, and point target amplitudes were generated separately and stored as MATLAB files for input into the simulation program. Within the simulation program, the transducer characteristics such as stave and row spacing were defined and focusing delays were calculated.

The simulated transducer was an array with an approximately circular aperture. The diameter was 10 cm, with a row spacing of 215.9 μm and a stave spacing of 254 μm. The simulated transducer impulse response was given by Fig. 4. The center frequency of the response was 4.74 MHz, calculated as $(f^+_{-3\text{ dB}}-f^-_{-3\text{ dB}})/2$, and the relative bandwidth was 82.5%. The lowest frequencies transmitted are below the -3-dB bandwidth; however, higher frequencies suffer greater attenuation. The transmitted signal was a linear FM chirp with frequency swept from 1 to 5 MHz, corresponding to steering angles of 24° to 5°. Simulating the actual data collection, a linear FM chirp was transmitted by the center two staves of the array.

The FIELD II program assumes a linear frequency dependence of attenuation, which is an appropriate assumption for tissue but not for water. In order to include attenuation in the

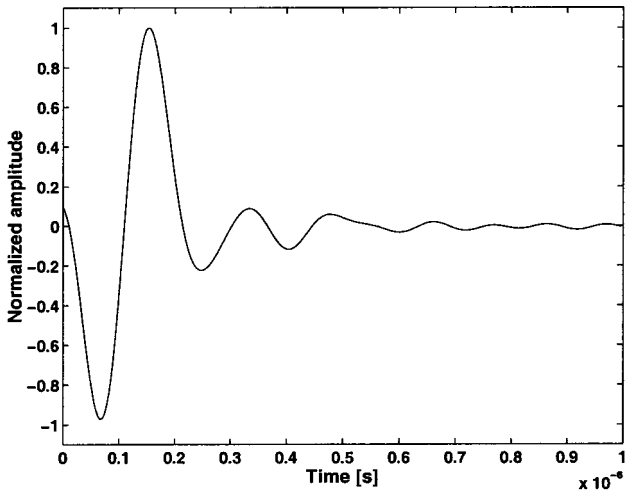

(a)

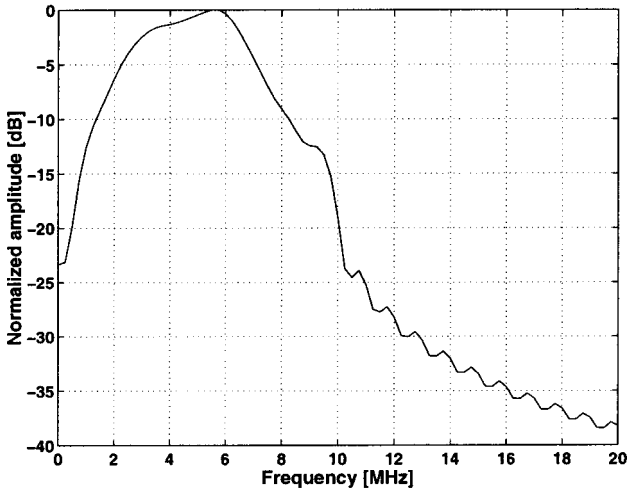

(b)

FIG. 4. Simulated transducer impulse response. The transducer has a center frequency of 4.74 MHz and an 82.5% bandwidth.

simulation, the target strengths were modified according to their range and vertical position, where vertical position determines the center frequency of the signal that will insonify the point. Attenuation was calculated using the equation for the plane-wave amplitude attenuation coefficient given by Tolstoy and Clay[23]

$$\alpha = \left(\frac{2.34\times 10^{-6} S f_T f^2}{f_T^2 + f^2} + \frac{3.38\times 10^{-6} f^2}{f_T} \right) \times (1 - 6.54\times 10^{-4} P), \tag{3}$$

where α is the attenuation coefficient in Np/m, $S=30$ is the salinity, given in parts per thousand, $P=1$ is the pressure in atm, $T=15°$ is the temperature in °C, $f_T = 21.9 \times 10^{6-1520/(T+273)} = 115.52$ is a frequency parameter given in kHz, and f is the operating frequency in kHz. Point target amplitudes were reduced according to the round-trip attenuation to that point. The target was placed at 4 m, centered at 0° horizontally and 10° vertically.

FIELD II was used to generate the received output voltage signal for each stave. The reflected signals were received by each of the elements in a stave, and the sum of the signals from elements in the same stave was calculated using the appropriate phase shift to simulate a lossless lens focused at 4 m in the vertical direction. The stave signals were stored in a matrix with stave number along one direction and time sample in the other direction. Before storing the time signal from a stave as one column of the matrix, appropriate time delays were implemented for focusing in the horizontal direction. Six depths of focus were used. They were 3.0, 3.3, 3.65, 4.0, 4.6, and 5.2 m.

Figure 3(b) shows how the four parts were combined to form an image. The $-j$ and -1 terms indicate phase shifts between the parts. Considering the array operating in receive mode, signals received on the sine channel must be phase shifted by $\pm 90°$ before combining them with signals received on the cosine channel in order to obtain the correctly steered beam. An identical phase shift is required on transmit. Therefore, a signal transmitted on the sine channel and received on the cosine channel requires a $\pm 90°$ phase shift. A signal transmitted on the cosine channel and received by the sine channel also requires a $\pm 90°$ phase shift. The sign of the 90° phase shift determines whether the beam is steered above or below broadside. A signal transmitted and received on the sine channel requires a 180° phase shift to be combined with the signal transmitted and received on the cosine channel.

B. Resolution analysis

Resolution analysis is performed by placing one simulated point target in the field at a time, and measuring the extent of the point spread function. Point targets were placed at 0° or 15° horizontally. Vertical positions ranged from 5° to 24° at 1-deg intervals. Range positions ranged from 3 to 5 m at 10-cm intervals. Range resolution is found using the time signal after the Radon transform for the correct horizontal steering direction. Envelope detection is performed using the Hilbert transform. Then, the envelope is log compressed and the points 6 dB below the maximum are found. The time difference between these points is then converted to distance using the speed of sound. Vertical resolution is found by first calculating the magnitude squared of the FFT of the entire received signal. Those data are then log compressed and the frequency values 6 dB below the maximum are found. That frequency information is then converted to angular information using[20]

$$\theta = \sin^{-1}\left(\frac{f_0 \sin\theta_0}{f} \right), \tag{4}$$

where θ is the steering direction for frequency f, θ_0 is the design steering angle, and f_0 is the design frequency. Finally, horizontal resolution is found by calculating the Radon transform for a range of angles around the target's actual angular position. This calculation forms part of an image in the horizontal angle/range plane. The horizontal resolution is the lateral extent of the point spread function measured by -6-dB points.

TABLE I. Horizontal resolution in degrees.

Vertical angle (deg)	Range (m) 3	3.5	4	4.5	5
5	0.239	0.237	0.231	0.237	0.238
7	0.332	0.335	0.329	0.322	0.316
9	0.429	0.432	0.427	0.419	0.407
11	0.525	0.527	0.521	0.465	0.457
13	0.619	0.575	0.570	0.565	0.559
15	0.710	0.710	0.704	0.700	0.694
17	0.810	0.811	0.806	0.802	0.799
19	0.907	0.911	0.907	0.902	0.900
21	0.983	0.981	0.974	0.970	0.966
23	1.082	1.081	1.079	1.078	1.076

Tables showing the results for horizontal, vertical, and range resolution for targets at 0° horizontally are given in Tables I, II, and III, respectively. Horizontal resolution stays fairly constant in range due to the multiple foci. Horizontal resolution degrades as vertical steering angle increases because lower frequencies are steered to larger angles. Vertical resolution degrades with range because only one focal zone is used. Vertical resolution degrades with increasing steering angle due to the change in frequency. Range resolution degrades slightly as range increases and it degrades as steering angle increases because of the change in frequency.

At very high frequencies (small steering angles), vertical resolution is better than horizontal resolution at closer ranges, but comparable to horizontal resolution at far ranges, because there is only one focus in the vertical direction. At low frequencies, vertical resolution is fairly stable because targets are in the far field, and therefore, focusing does not have any effect. Also, for low frequencies vertical resolution is better than horizontal resolution because of the transmit–receive combination. The transmit beam pattern is wide in the horizontal direction, but narrow in the vertical direction. The main lobe of the receive beam pattern is narrow both in the horizontal and vertical directions. The comparison between vertical and horizontal resolution shows one of the advantages of the amplitude-steered array over a system that uses a broad transmit and a conventional phased array to receive. Better resolution in the vertical direction than in the horizontal direction is a result of having a narrow transmit beam in the vertical direction for each frequency.

TABLE II. Vertical resolution in degrees.

Vertical angle (deg)	Range (m) 3	3.5	4	4.5	5
5	0.151	0.178	0.310	0.260	0.213
7	0.221	0.231	0.244	0.275	0.340
9	0.283	0.292	0.301	0.317	0.333
11	0.338	0.344	0.356	0.363	0.373
13	0.403	0.407	0.413	0.418	0.426
15	0.521	0.526	0.537	0.547	0.555
17	0.547	0.549	0.556	0.561	0.563
19	0.643	0.648	0.653	0.658	0.664
21	0.688	0.701	0.698	0.706	0.710
23	0.766	0.773	0.778	0.780	0.788

TABLE III. Range resolution in mm.

Vertical angle (deg)	Range (m) 3	3.5	4	4.5	5
5	4.76	5.42	3.52	3.52	3.66
7	6.34	7.03	7.62	8.13	8.31
9	8.09	8.75	9.38	9.78	10.1
11	9.96	10.5	11.1	11.6	11.9
13	12.0	12.5	13.0	13.5	13.8
15	13.0	13.5	14.2	14.6	15.1
17	15.5	15.9	16.3	16.7	17.0
19	16.8	17.4	17.9	18.3	18.7
21	18.8	19.2	19.5	19.9	20.1
23	20.3	20.9	21.1	21.5	21.8

Resolutions are also measured for data following time–frequency processing. In this case, only range and vertical resolutions are measured. The Radon transform is calculated for the appropriate steering angle, then two-dimensional images are formed using either the spectrogram or the SPWD. The comparison is thus made for slice images at one horizontal steering direction rather than for projections through the horizontal steering direction. Resolutions are measured from the image as the −6-dB range and vertical extent of the pulse spread function.

Plots showing the comparisons of range and vertical resolutions for the case of no time–frequency processing or processing with the spectrogram and SPWD are given in Fig. 5. Part (a) shows the range resolutions for the three cases. The solid line respresents the results for no processing, and should be the lowest line for all angles. However, the dotted line, representing the results for the SPWD, dips below the solid line. The SPWD can produce resolution very close to the limit of no processing, but it cannot do better. Part (b) shows the results for the vertical resolution. Again, the SPWD resolution approaches that of no processing.

For both range and vertical resolution, the spectrogram results are not as good as the others. We could improve one at the expense of the other by changing the window length. For comparison, in (b), the dashed-dotted line shows the horizontal resolution measured with no processing. It is worse than the resolution in the vertical direction because the transmit beam in the horizontal direction is broad.

C. Simulated target

To demonstrate the array operation, projection images were produced by simulating data collection from a more complicated target. The target used for these simulations was designed to include some features of a mine, including representations of bolts and a slanted face. A diagram of the target with dimensions is shown in Fig. 6. The bolts are approximately 2 cm across and raised 1 cm above the planar surface of the mine to test the resolution limits. The slanted face is intended to provide information about depth resolution. The original computer model of this target was created at the Applied Research Laboratory at the Pennsylvania State University using AUTOCAD. In this study, we use the model by assuming the node positions of AUTOCAD were point tar-

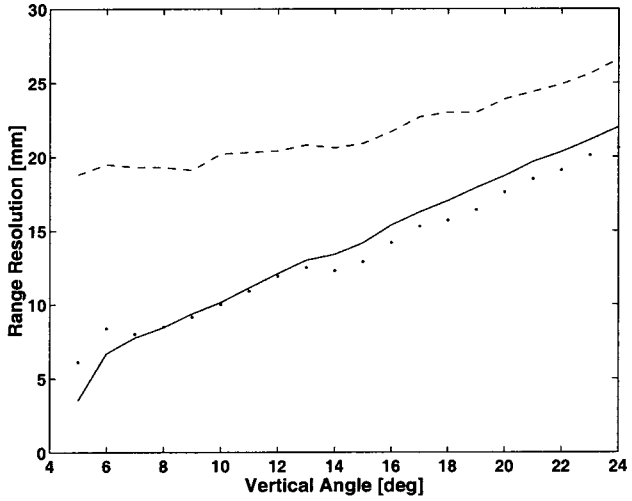

(a)

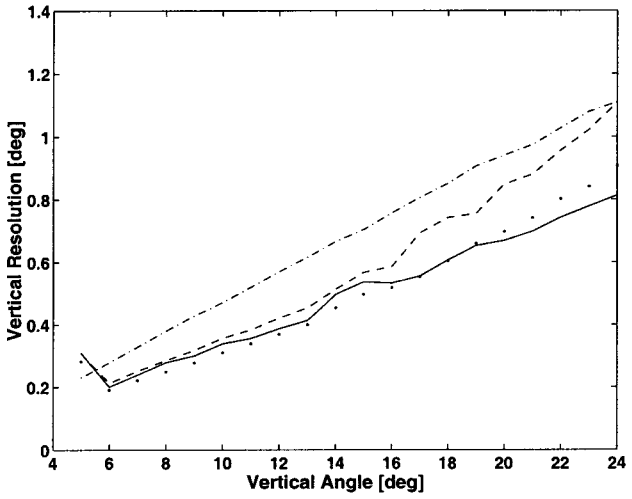

(b)

FIG. 5. Comparison of resolutions for no processing (solid line), spectrogram processing (dashed line), and SPWD processing (dotted line), for (a) range resolution and (b) vertical resolution. For comparison, the dashed-dotted line in (b) shows the horizontal resolution measured with no processing.

gets in the FIELD II program. The definition of the bolts required many nodes. Therefore, they were highly dense targets, making them easier to detect.

The point-target representation of the target is shown in Fig. 7. The orientation of the target in these figures corresponds to the orientation in which it is imaged. The axis labeled *X-Lateral direction* corresponds to horizontal steering directions. The axis labeled *Y-Lateral direction* corresponds to vertical steering angles. *Height* corresponds to axial distance. The bolts are closest to the array in range.

D. Image results

Sample projection images are shown in Figs. 8, 9, 10, and 11. In each of these projection images, one dimension of resolution that is present in the data is given up to display the image.

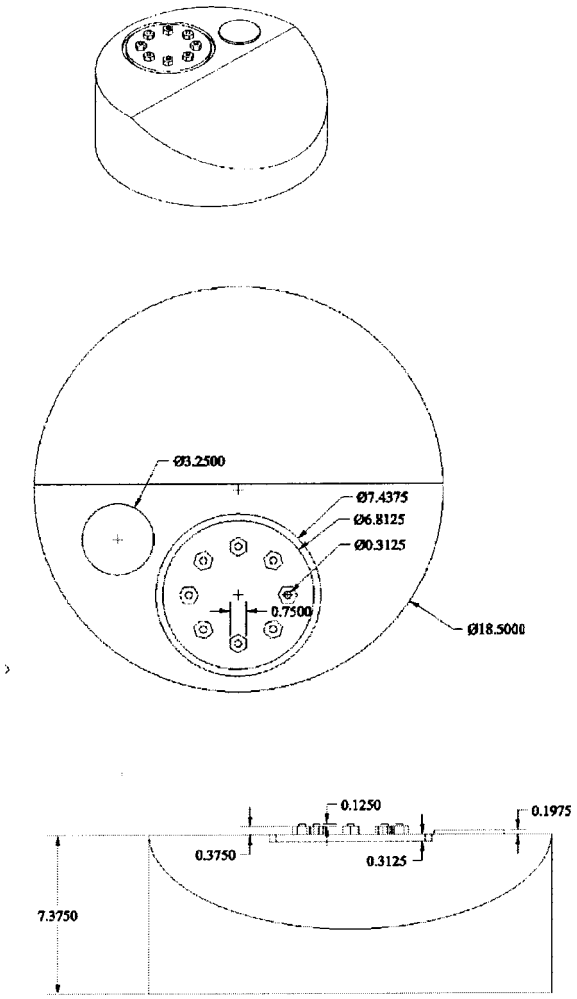

FIG. 6. Diagram of test target. Dimensions are given in inches.

Figure 8 shows the projection image through the vertical direction or the view from the top. At this orientation, which corresponds to Fig. 7(b), the observer sees the cylindrical target along its height; therefore, it appears as a rectangle. The bolts appear as white spots at the top of the image which corresponds to the closest range. Figure 9 shows the projection through range or the front view. This is a C-mode image in that the plane of view is parallel to the plane containing the transducer. At this orientation, which corresponds to Fig. 7(a), the observer views the top of the cylinder, so that the target appears as a circle. The slanted face is not apparent in the projection image. It is apparent in an image displaying the range of the first maximum (not shown). The bolts appear as a ring of bright spots near the bottom of the circle. The bottom of the circle, which corresponds to higher frequencies, appears more dim due to the greater attenuation despite the better frequency response of the transducer at higher frequencies. The top of the circle, corresponding to lower incident frequencies, appears more blurred due to the wider beamwidths at lower frequencies.

Figures 10 and 11 show the projection through the horizontal direction or the side view. Figure 10 uses the spectrogram to calculate the projection, and Fig. 11 uses the SPWD. In both cases, the bottom of the image is more dim and the top is more blurred for the reasons discussed above. Also in

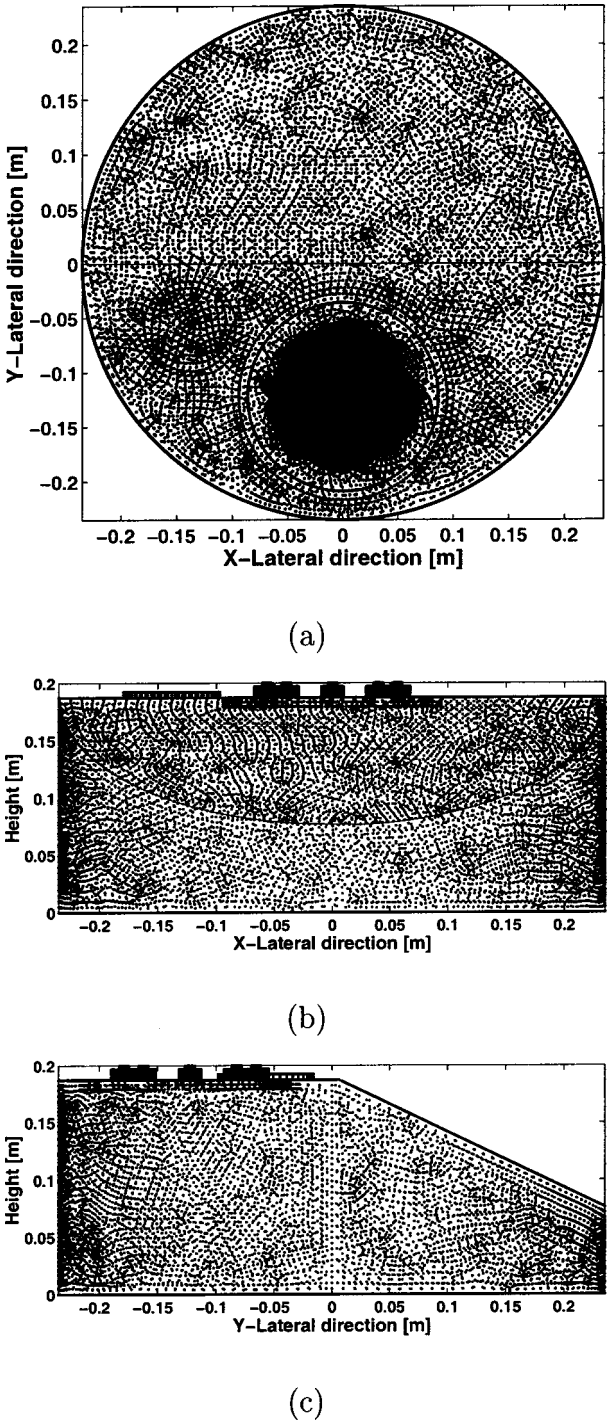

FIG. 7. View of target as point sources: (a) top; (b) from horizontal, with the sloped surface facing the reader; and (c) from vertical.

both cases, the overall shape of the target with the slanted face in the vertical direction is apparent. The SPWD image is much sharper than the spectrogram image. The SPWD image suffers from streaking in the vertical direction. The streaking can be reduced at the expense of resolution in the vertical direction by increasing the smoothing in that direction.

The three projection images allow us to display the data with reduced processing. Together, the three projection images produce an impression of the shape of the target. Resolution of small features can be improved by increasing the diameter of the array. Resolution may also be improved by increasing the frequency; however, increasing the frequency may cause additional problems due to the increase in attenuation.

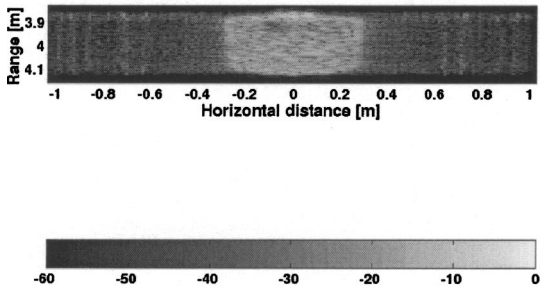

FIG. 8. Projection through the vertical direction, formed by envelope-detecting data following the Radon transform. The gray scale is in dB.

V. DISCUSSION

We have shown that by using frequency steering in one direction, the lateral resolution is improved in that direction, over the resolution achieved using a wide transmit beam. To improve resolution in both directions, we would like to be able to transmit a single pulse, using the full array rather than two staves, and then form images using frequency steering in both vertical and horizontal directions. We would consider this the full two-dimensional amplitude-steered array. Our current system for volumetric imaging is more accurately described as a linear-phased amplitude-steered array, because amplitude steering is used in the vertical direction, and conventional phased-array beam steering is used in the horizontal direction.

We are not able to achieve the full two-dimensional amplitude-steered array by applying fixed amplitude weighting along both rows and staves. With amplitude weighting only in the vertical direction, and assuming no phased-array steering in the horizontal direction, a pulse collects a plane of data perpendicular to the array face that is vertical. If we applied fixed amplitude weighting in both vertical and horizontal directions, a single pulse would produce a two-dimensional image representing a plane perpendicular to the array face and rotated around the array axis.

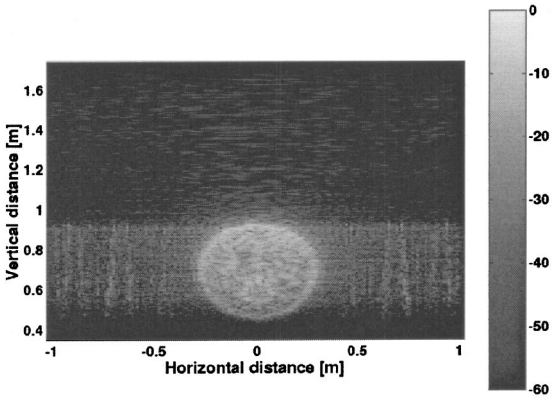

FIG. 9. Projection through the range direction, formed by calculating the Fourier transform of each signal following the Radon transform. The gray scale is in dB.

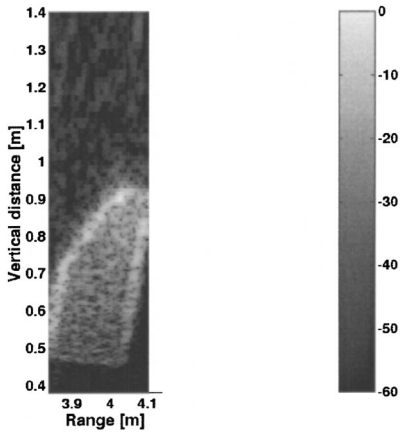

FIG. 10. Projection through the horizontal direction, formed using the spectrogram processing on the summed output of the Radon transform. The gray scale is in dB.

Lu's array, which forms *grid array beams*, could be considered a full two-dimensional amplitude-steered array, in that array weighting is used in both lateral directions. However, his amplitude weighting is not fixed. An extensive bibliography of Lu's work in limited diffraction beams is available in Ref. 11.

Forming grid array beams requires amplitude weighting on the elements of a two-dimensional array which is derived from Eq. (11) of Ref. 24:

$$\Phi_G(x,y,z-c_1t)=(\cos k_x x)(\cos k_y y)e^{ik_z(z-c_1t)}, \tag{5}$$

where Φ_G is a three-dimensional wave field, the subscript G refers to grid array beams, x and y are the lateral directions, z is the axial direction, and (k_x, k_y, k_z) are the components of the vector wave number. Equation (5) is a limited diffraction solution to the wave equation because the transverse beam pattern does not change as z increases. The weighting on the elements is given by

$$A(x,y)=\cos(k_x x)\cos(k_y y). \tag{6}$$

Choosing values for the parameters k_x and k_y gives one set of grid array beams, and therefore, one received signal. That single signal cannot be processed by itself to give target position in three dimensions. Multiple grid array beams are formed in order to obtain the data for target localization. Forming an image requires changing the weighting on the elements by changing k_x and k_y. By calculating the output of the array for many different values of k_x and k_y, i.e., summing signals from array elements with different weightings, a three-dimensional data set is formed. Multiple sets of beams can be formed by storing signals from individual elements of the transducer array or by using electronics to calculate multiple grid array beams, and therefore multiple received signals, at once. The image is obtained using a three-dimensional inverse Fourier transform.

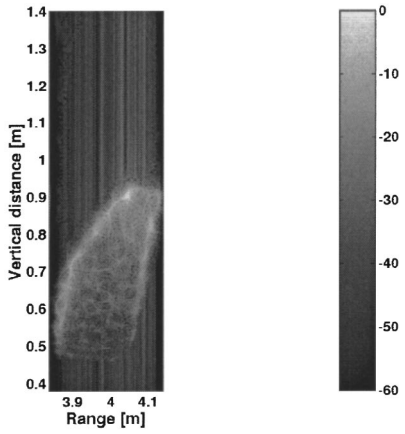

FIG. 11. Projection through the horizontal direction, formed using SPWD processing on the summed output of the Radon transform. The gray scale is in dB.

We can put our amplitude weighting in the form of Eq. (5); however, our weighting is only in the x direction, and it is fixed. For each row, we have weighting terms $\cos((2n-1)\phi)$ and $\sin((2n-1)\phi)$, where n was an index used to enumerate the row and $\phi=(k_0 d/2)\sin\theta_0$. These weighting terms are discretized versions of $\cos(k_x x)$ and $\sin(k_x x)$, where $k_x=k_0\sin\theta_0$ and $x=(2n-1)(d/2)$. With fixed weighting, we have only a single value of k_x, whereas the limited diffraction beam system uses variable k_x and k_y. The result is that our lateral resolution varies with angle. Lu's lateral resolution remains constant at a particular range.

One final difference between our work and that of Lu is that, although we apply similar weighting to our array, we do not claim to be using limited diffraction beams. For a finite array size, the transmitted and receive beams will diffract; however, Lu forms his images well within the near field and finds that diffraction effects are not important. We form our images before the near-field/far-field transition for part of our frequency range; however, for the lower frequencies, our targets are assumed to be in the far field of the array.

VI. CONCLUSIONS

We have introduced the linear-phased amplitude-steered array and associated processing for real-time volumetric imaging.[25] A previous implementation of the amplitude-steered array suffered from grating lobes and large beamwidths. The array layout has been modified with randomized element assignment so that sidelobes are low. And, the aperture is large compared with a wavelength even at the lowest frequency, so the beamwidths have been improved.

The main obstacle to collecting a volume of high-resolution, high SNR data in real time is the time required to scan a beam in two dimensions. Often, to avoid scanning the transmit beam in many directions, a broad transmit beam is used; however, the result is poorer resolution than would be achieved by using a narrow transmit and receive beam. Using the amplitude-steered array, the beam, which is narrow in the vertical dimension, is scanned in the vertical direction as the frequency of the transmitted pulse changes. Received signals from different directions are separated by frequency content, not by time, greatly reducing the time required to collect data and with improved lateral resolution in the direction of frequency separation. The amplitude-steered array offers the additional benefit of reducing the number of channels required to process data from a dense two-dimensional array. The array uses only four channels per column of elements rather than one channel for each array element.

We chose to transmit a broad beam in the horizontal direction and to focus in that dimension only on receive because the large ranges associated with our application required collecting a volume of data with a single transmit pulse. For medical imaging, with shorter ranges of interest and greater demand for high resolution, we could transmit beams that are narrow and steered in the horizontal direction as well as in the vertical direction. The volume of data would be collected in the same time that it currently takes to form a two-dimensional image using standard ultrasonic imaging techniques.

ACKNOWLEDGMENTS

The authors would like to thank Scott Brown and Dave van Tol of ARL for developing the random array layout, Paul G. Bednarchik for developing the AUTOCAD model of the simulated target, and Chuck Allen for coordinating the research effort. We would also like to acknowledge the support of Bruce Johnson and DARPA and to thank the anonymous reviewers whose comments greatly improved the presentation of this work.

[1] W. J. Hughes and W. Thompson, Jr., ''Tilted directional response patterns formed by amplitude weighting and a single 90° phase shift,'' J. Acoust. Soc. Am. **59**, 1040–1045 (1976).
[2] W. J. Hughes, W. Thompson, Jr., and R. D. Ingram, ''Transducer array scanning system,'' United States Patent 3,905,009, 9 Sept. 1975.
[3] W. J. Hughes and C. W. Allen, ''A shaped PVDF hydrophone for producing low sidelobe beampatterns,'' Proceedings of the 1992 Symp. on Autonomous Underwater Vehicle Technology, 2–3 June 1992, Washington, D.C.
[4] W. J. Hughes and C. W. Allen, ''A spatially phased transducer to form steered beams,'' Proceedings of SPIE, Medical Imaging 1999: Ultrasonic Transducer Engineering **3664**, 138–146 (1999).
[5] C. H. Frazier, W. J. Hughes, and W. D. O'Brien, Jr., ''Volumetric imaging with an amplitude-steered array,'' J. Acoust. Soc. Am. **112**, 2753–2762 (2002).
[6] T. R. Nelson and D. H. Pretorius, ''Three-dimensional ultrasound imaging,'' Ultrasound Med. Biol. **24**(9), 1243–1270 (1998).
[7] S. Berg, H. Torp, D. Martens, E. Steen, S. Samstad, I. Høivik, and B. Olstad, ''Dynamic three-dimensional freehand echocardiography using raw digital ultrasound data,'' Ultrasound Med. Biol. **25**(5), 745–753 (1999).
[8] R. Canals, G. Lamarque, and P. Chatain, ''Volumetric ultrasound system for left ventricle motion imaging,'' IEEE Trans. Ultrason. Ferroelectr. Freq. Control **46**(6), 1527–1538 (1999).
[9] S. W. Smith, H. G. Pavy, Jr., and O. T. von Ramm, ''High-speed ultrasound volumetric imaging system. I. Transducer design and beam steering,'' IEEE Trans. Ultrason. Ferroelectr. Freq. Control **38**(2), 100–108 (1991).
[10] J.-Y. Lu, ''2D and 3D high frame rate imaging with limited diffraction beams,'' IEEE Trans. Ultrason. Ferroelectr. Freq. Control **44**(4), 839–856 (1997).
[11] J.-Y. Lu, ''Experimental study of high frame rate imaging with limited diffraction beams,'' IEEE Trans. Ultrason. Ferroelectr. Freq. Control **45**(1), 84–97 (1998).
[12] J. Shen and E. S. Ebbini, ''A new coded-excitation ultrasound imaging system. I. Basic principles,'' IEEE Trans. Ultrason. Ferroelectr. Freq. Control **43**(1), 131–140 (1996).
[13] B. D. Steinberg, ''Comparison between peak sidelobe of the random array and algorithmically designed aperiodic arrays,'' IEEE Trans. Antennas Propag. **AP-21**(3), 366–370 (1973).
[14] B. D. Steinberg, ''The peak sidelobe of the phased array having randomly located elements,'' IEEE Trans. Antennas Propag. **AP-20**(2), 129–136 (1972).
[15] D. H. Johnson and D. E. Dudgeon, *Array Signal Processing: Concepts and Techniques* (Prentice-Hall, Englewood Cliffs, NJ, 1993).
[16] P. Chevret, N. Gache, and V. Zimpfer, ''Time-frequency filters for target classification,'' J. Acoust. Soc. Am. **105**, 3168–3175 (1999).
[17] L. R. Dragonette, D. M. Drumheller, C. F. Gaumond, D. H. Hughes, B. T. O'Connor, N.-C. Yen, and T. J. Yoder, ''The application of two-dimensional signal transformations to the analysis and synthesis of structural excitations observed in acoustical scattering,'' Proc. IEEE **84**(9), 1249–1263 (1996).
[18] L. Cohen, ''Time–frequency distributions—A review,'' Proc. IEEE **77**(7), 941–981 (1989).
[19] C. H. Frazier and W. D. O'Brien, Jr., ''Image formation with the amplitude-steered array using time–frequency processing,'' Acoust. Imaging **25**, 535–542 (2000).
[20] C. H. Frazier, W. J. Hughes, and W. D. O'Brien, Jr., ''Resolution analysis for an amplitude steered array,'' J. Acoust. Soc. Am. **107**, 2430–2436 (2000).
[21] J. A. Jensen, ''FIELD: A program for simulating ultrasound systems,'' Med. Biol. Eng. Comput. **34**(1), Suppl. 1, 351–353 (1996).
[22] Program is available at http://www.it.dtu.dk/~jaj/field/field.html
[23] I. Tolstoy and C. S. Clay, *Ocean Acoustics: Theory and Experiment in Underwater Sound* (McGraw-Hill, St. Louis, 1966).
[24] J.-Y. Lu, ''Limited diffraction array beams,'' Int. J. Imaging Syst. Technol. **8**(1), 126–136 (1997).
[25] C. A. H. Frazier, ''A two-dimensional amplitude-steered array for real-time volumetric acoustic imaging,'' Ph.D. thesis, University of Illinois at Urbana-Champaign, 2000.